A Low-Complexity Standard-Compliant PAPR Reduction Scheme for OTFS Modulation

Salil Sharma*†, *Member, IEEE*, Syed Waqas Haider Shah*, *Member, IEEE*, and Joerg Widmer*, *Fellow, IEEE*

*IMDEA Networks Institute, Madrid, Spain
† Universidad Carlos III de Madrid, Madrid, Spain
{salil.sharma, syed.waqas, joerg.widmer}@imdea.org

***Abstract*—Orthogonal Time Frequency Space (OTFS) modulation is widely recognized as a modulation scheme with advantageous properties for both radar and communication waveform designs. In OTFS, information symbols are mapped in the Delay-Doppler (DD) domain leading to reliable communication in high Doppler channels. However, the presence of inverse-discrete Fourier Transform operation in OTFS architecture results in a high Peak-to-Average Power Ratio (PAPR) in the transmit OTFS frames. This paper introduces a novel metric-based symbol pre-distortion algorithm constrained by Error Vector Magnitude (EVM) limits to reduce the PAPR in OTFS modulation. The imposed constraint in the form of EVM limits establishes it as a pragmatic method that adds no side-channel information rather exploits the available EVM limit usually kept in wireless standards. The pre-distortion applied to each symbol/sample in an OTFS frame is determined by the proposed metrics, representing the contribution of each symbol to peak values in the output. The proposed method is simple, flexible, and does not require additional complexity for symbol detection on the receiver end. Our simulation results demonstrate a significant reduction in the PAPR of OTFS blocks for both QPSK and 16-QAM modulation schemes. Furthermore, our proposed Constrained Constellation Shaping scheme exhibits enhanced performance in PAPR reduction as the number of Doppler bins increases for an OTFS frame size.**

***Index Terms*—Orthogonal Time Frequency Space, Peak-to-Average Power Ratio, Constellation Shaping, Error Vector Magnitude**

I. Introduction

As we swiftly advance toward the future of wireless communication technologies, a significant challenge lies in addressing high-Doppler wireless scenarios. Orthogonal Time Frequency Space (OTFS) modulation has garnered considerable attention due to its capacity to enable reliable communication in high Doppler channels [1]–[6]. OTFS modulation maps information symbols in the form of a matrix in the Delay-Doppler (DD) domain and transforms the time-varying multipath channel in the Time-Frequency (TF) domain into a time-invariant and sparse channel in the DD domain. This representation allows for reliable and robust communication in high-Doppler environments.

The potential of OTFS for radar applications has been discussed in [7], highlighting its efficiency in high-Doppler radar scenarios. Efficient OTFS transmitter designs using inverse-discrete Zak Transform (DZT) have been explored in [8], [9], and the practical application of OTFS architecture for pulse-Doppler radar has been investigated in [10]. These studies collectively underscore OTFS as an exceptional candidate for future communications, radar, and integrated sensing and communication applications.

However, along with its advantages, OTFS modulation, like other multicarrier modulations, faces challenges such as a high peak-to-average-power ratio (PAPR). In [11], authors provide a PAPR bound for OTFS modulation, demonstrating that PAPR grows linearly with an increase in Doppler bins or sub-pulses, in contrast to other multicarrier waveforms where PAPR grows linearly with the number of subcarriers. Strategies for PAPR reduction in OTFS are presented in [12]–[14], involving techniques such as indexing, frame-structuring, and precoding. While effective in reducing PAPR, these designs often require additional side-channel information at the receiver. To circumvent the need for transmitting side-channel information, authors in [15]–[17] propose metric-based symbol pre-distortion strategies to address PAPR. It is worth noting that these strategies are specifically tailored for OFDM modulation and may not be directly applicable to OTFS modulation.

These investigations collectively underscore the significance of tackling PAPR challenges in OTFS modulation, particularly for its broader applicability in high-Doppler wireless scenarios. However, to the best of the authors' knowledge, there are no prior works addressing the PAPR challenge of OTFS modulation without introducing any side-channel information while also ensuring compliance with wireless standards.

To address this challenge, our paper introduces a novel metric-based symbol pre-distortion method tailored for OTFS modulation to effectively reduce PAPR. In our proposed method, a metric is computed for each input information symbol, determining the magnitude and direction of the pre-distortion required to minimize PAPR. These computed metrics guide the determination of pre-distortion values, aligning with EVM constraints that can be empirically chosen based on system design considerations. In practical terms, wireless standards stipulate EVM limits for various modulation schemes during transmit-side processing. The proposed method offers a one-shot PAPR reduction strategy for OTFS modulation, providing robust control over pre-distortion and ensuring compatibility with existing and potential future standards incorporating OTFS modulation. Our simulation results demonstrate the efficacy of the proposed method in reducing the PAPR by

up to 2 dB, while meeting the specified EVM constraints.

II. OTFS Modulation

In this section, we provide a concise overview of OTFS modulation. The fundamental principle of OTFS modulation involves transmitting data or information symbols across the DD domain of a wireless channel. This is achieved by mapping information symbols from the DD grid to the TF grid, followed by the application of a generalized Orthogonal Frequency Division Multiplexing (OFDM) modulation over the samples in the TF grid [10]. In Fig. 1, we depict a basic transmitter schema for an $N \times M$ size OTFS frame, where N represents delay-taps or subcarriers, and M denotes Doppler-bins or subpulses. The incoming information symbol train, such as Quadrature Amplitude Modulation (QAM) or Phase Shift Keying (PSK) symbols, is converted to a matrix of dimensions $N \times M$ using a Serial-to-Parallel conversion block (S/P). We use $\mathbf{X_{DD}}$ to represent the information block of an OTFS frame, and $a_{k,l}$ denotes the symbol at the k^{th} delay and l^{th} Doppler bin. Next, $\mathbf{X_{DD}}$ undergoes a transformation from the DD domain to the Time-Frequency domain using the Inverse Symplectic Finite Fourier Transform (ISFFT). This is followed by a generalized OFDM modulation, where samples are transformed from the Time-Frequency domain to the Delay-Time (DT) domain. Subsequently, the result is parallel-to-serial (P/S) converted to obtain the OTFS transmit frame vector. The expression for the transmit OTFS frame vector S is given as

$$S = vec(\mathbf{F_N}^{\mathbf{H}}\mathbf{F_N}\mathbf{X_{DD}}\mathbf{F_M}^{\mathbf{H}}), \tag{1}$$

where $\mathbf{F_N}$ and $\mathbf{F_M}$ represent Fourier matrices with dimensions $N \times N$ and $M \times M$, respectively. The operation $(\cdot)^H$ denotes the Hermitian operation. This equation can be further simplified as expressed in the following

$$S = vec(\mathbf{X_{DT}}) = vec(\mathbf{X_{DD}}\mathbf{F_M}^{\mathbf{H}}), \tag{2}$$

where $\mathbf{X_{DT}}$ is the OTFS frame in the DT domain. The output time-domain samples are described by

$$s(k+mN) = \sum_{l=0}^{M-1} a_{k,l} e^{j2\pi m \frac{l\Delta f T_c}{M}}, \tag{3}$$

where $s(k+mN)$ is the $k+mN$-th sample, $a_{k,l}$ represents the symbol at the k^{th} delay and l^{th} Doppler bin, $j = \sqrt{-1}$ is the imaginary unit, and $k = \{0, \cdots, N-1\}$, $l = \{0, \cdots, M-1\}$, and $m = \{0, \cdots, M-1\}$ are the sampling indices for delay-bin or subcarrier and Doppler-bin or subpulse, respectively. The sampling time of each chip is denoted as T_c, and $\Delta f = \frac{1}{T_c}$ represents the inter-spacing between subcarriers (for OTFS).

This mathematical representation offers a comprehensive insight into the OTFS modulation process, where symbols are efficiently transmitted across the DD domain, and the resulting time-domain samples are precisely characterized by the specified equations. Next, we discuss the PAPR of an OTFS waveform.

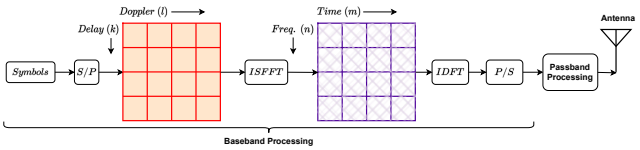

Fig. 1: Transmitter schematic of OTFS waveform for N delay-bins/subcarriers and M Doppler-bins/subframes.

A. PAPR in OTFS Modulation

For a discrete version of an OTFS waveform, the PAPR is defined as the following

$$\text{PAPR} = \frac{\max_i |s(i)|^2}{\frac{1}{NM}\sum_{i=0}^{NM-1}|s(i)|^2}, \tag{4}$$

where $s(i)$ represents the i^{th} sample in the OTFS frame. Similar to other multicarrier waveforms, OTFS also exhibits high PAPR. However, in the case of OTFS waveforms, the PAPR grows linearly with an increase in Doppler bins or subpulses (M), contrasting with other multicarrier waveforms where the PAPR grows linearly with the number of subcarriers (N) [11]. This distinction arises because peak samples are formed due to an Inverse Fourier transformation, and in the case of OTFS, the transform occurs along the dimension of Doppler bins rather than the subcarriers.

B. Constellation Error Vector Magnitude

For any given transmit OTFS frame vector with noise or distortion, there is a resulting distortion in the information symbols from their ideal constellation symbols. Let $c_o \in \mathbb{C}^n$ denote the ideal constellation of the information symbols, and $c_d \in \mathbb{C}^n$ represent the actual constellation of the transmit symbols. The root-mean-squared EVM (ϵ_{rms}) of c_d is defined as [18]:

$$\epsilon_{rms} = \sqrt{\frac{\sum_{i=0}^{NM-1}|c_{di} - c_{oi}|^2}{NM}} \tag{5}$$

Here, Eq. (5) quantifies the root-mean-squared EVM, providing a measure of the discrepancy between the actual and ideal constellations, reflecting the impact of noise or distortion in the transmitted OTFS frame. A transmission adhering to the EVM constraint ensures that the received data achieves a satisfactory Bit Error Rate (BER). The permissible maximum EVM is typically determined empirically, and is commonly specified in different wireless communication standards, e.g., [18].

III. Proposed Metric-Based Constrained Constellation Shaping

In this section, we introduce a novel metric-based constrained constellation shaping (CCS) method designed to reduce the PAPR of an OTFS waveform while adhering to EVM constraints. The known metric-based predistortion techniques in [15]–[17] introduce the concept of metric computation for OFDM but exploit it only to perform Active Constellation Extension of some or a set of transmit symbols. Some of these techniques are iterative in nature and do not address

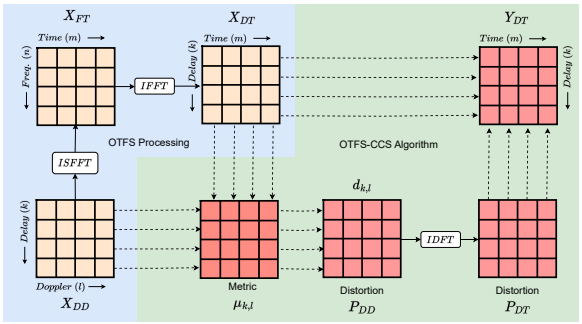

Fig. 2: Schematic workflow of the OTFS processing and Constrained Constellation Shaping in OTFS modulation based on metric computation.

issues like EVM compliance. On the other hand, the proposed method distinguishes itself as a one-shot solution for OTFS modulation, in which metrics are used for CCS. These metrics are constrained by the EVM margin and also without the need for any side-channel information.

A comprehensive overview of the proposed method is given in Algorithm 1 and shown in Fig. 2, with subsequent subsections delving into the details of each stage. Here $\mathbf{X_{DD}}$, $\mathbf{X_{FT}}$ and $\mathbf{X_{DT}}$ are the transmit OTFS frame in DD domain, Time-Frequency domain and DT domain respectively. $\mathbf{Y_{DT}}$ represents the updated OTFS frame with reduced PAPR in DT domain.

In Fig. 2, the OTFS transmit-side processing part performs the processing of information symbols from the DD domain into the Time-Frequency domain and then to the DT domain. These delay-time domain symbols help us find the metrics for the pre-distortion of symbols. We propose computing metrics for each symbol $a_{k,l}$ as $\mu_{k,l}$ by utilizing samples from both $\mathbf{X_{DD}}$ and $\mathbf{X_{DT}}$, this is discussed in detail in the subsequent subsection. The metric values assigned to each $a_{k,l}$ highlight the impact of each symbol on the peak samples in $\mathbf{X_{DT}}$. This insight provides guidance on the extent of relative distortion that should be applied to each $a_{k,l}$ within each row of $\mathbf{X_{DD}}$ and the corresponding direction of distortion. One approach involves scaling each metric row in the matrix of metric values and adjusting the distortion direction to generate a matrix of pre-distortion samples. However, since these samples are generated with respect to $a_{k,l}$, such pre-distortion remains in the DD domain.

Subsequently, the $\mathbf{P_{DD}}$ matrix of pre-distortion samples undergoes transformation to its DT counterpart, $\mathbf{P_{DT}}$, through an IDFT operation along the Doppler dimension. Upon addition to $\mathbf{X_{DT}}$, this generates $\mathbf{Y_{DT}}$, representing the updated OTFS frame with reduced PAPR. The addition of distortion in the DT domain, i.e., $\mathbf{Y_{DT}} = \mathbf{X_{DT}} + \mathbf{P_{DT}}$, also implies the addition of distortion in the DD domain, where $\mathbf{Y_{DD}} = \mathbf{X_{DD}} + \mathbf{P_{DD}}$. In this context, $\mathbf{Y_{DD}}$ signifies the updated information symbols, now incorporating pre-distortion, in the DD domain. A well-calibrated computation of metrics and pre-distortion samples leads to constrained constellation shaping of information symbols within the DD grid, aligned with the chosen EVM threshold. Simultaneously, in the DT grid, it implies a reduction in the amplitude of peak values compared to the original frame $\mathbf{X_{DT}}$, thereby resulting in a decreased PAPR in the updated frame $\mathbf{Y_{DT}}$.

Algorithm 1: CCS-based PAPR reduction for OTFS modulation

Input: $s[i]$ (symbol-train), OTFS frame (N delay-bins, M Doppler-bins), ϵ_{rms} (EVM threshold), p (for weight computation)
Output: $y[i]$ Output OTFS waveform
Step-I: Convert symbol-train $s(n)$ to X_{DD} of dimension $N \times M$ using;
for $n \leftarrow 1$ **to** N **do**
  for $m \leftarrow 1$ **to** M **do**
    $X_{DD}(n,m) \leftarrow s[n+(m-1)N]$;
  end
end
Step-II: Generate X_{DT} using Eq. (2);
Step-III: Compute metrics $\mu_{k,l}$ using Eq. (8);
Step-IV: Compute P_{DD} using Eq. (9);
Step-V: Obtain Y_{DT} using Eq. (10);
Step-VI: Convert Y_{DT} to the output sample-train $y(i)$ using;
for $n \leftarrow 1$ **to** N **do**
  for $m \leftarrow 1$ **to** M **do**
    $y[n+(m-1)N] \leftarrow Y_{DT}(n,m)$;
  end
end

A. Metric Computation

In our proposed method, our primary objective is to reduce the power of peak samples contributing to a higher PAPR, while preserving symbols from pre-distortion that inherently have low contribution to peak samples. As a result, our initial step involves computing metrics that serve as a relative indication of which symbols in each row of $\mathbf{X_{DD}}$ necessitate pre-distortion and in which direction to effectively reduce the overall PAPR of the OTFS frame. Additionally, we introduce a weighting function that takes into account the peak power values associated with each symbol. This weighting function plays a pivotal role in selectively weighing samples with relatively high power values in the DT domain of the OTFS frame.

From Eq. (2), the derivation of $\mathbf{X_{DT}}$ involves performing the IDFT on each row of $\mathbf{X_{DD}}$. The influence of each symbol $a_{k,l}$ on the corresponding output $b_{k,m}$(s) can be expressed as $a_{k,l}e^{j2\pi ml/M}$. A generalized form of the metric pertaining to the symbol $a_{k,l}$ within $\mathbf{X_{DD}}$ is defined as follows:

$$\mu_{k,l} = \sum_{m=0}^{M-1} g(b_{k,m}, a_{k,l}) v(b_{k,m}), \tag{6}$$

where $g(\cdot)$ represents a function that provides the negative projection between $b_{k,m}$ and $a_{k,l}e^{j2\pi ml/M}$, while $v(\cdot)$ is a

function specifying the weight for each sample of $\mathbf{X_{DT}}$. A considerable choice for the weight function is $v(b_{k,m}) = |b_{k,m}|^p$, which is the p^{th} norm of $b_{k,m}$. Consequently, the metric is the sum of the weighted negative projections of all output symbols for a given input symbol. The function $g(b_{k,m}, a_{k,l})$ is defined as $g(b_{k,m}, a_{k,l}) = -\cos(\phi_{b_{k,m},a_{k,l}})$, where $\cos(\phi_{b_{k,m},a_{k,l}})$ represents the angular projection between $b_{k,m}$ and $a_{k,l}$. This angular projection is given by the following expression

$$\cos(\phi_{b_{k,m},a_{k,l}}) = \Re\left\{\frac{b_{k,m}{a^*}_{k,l}e^{-j2\pi lm/M}}{|b_{k,m}||a_{k,l}|}\right\}, \tag{7}$$

where $\Re(\cdot)$ denotes the real part of a complex number. Next, by substituting Eq. (7) in Eq. (6) , the final expression for the metric $\mu_{k,l}$ becomes

$$\mu_{k,l} = \frac{-1}{|{a^*}_{k,l}|}\sum_{m=0}^{M-1}\Re\left\{{a^*}_{k,l}b_{k,m}|b_{k,m}|^{p-1}e^{-j2\pi lm/M}\right\}. \tag{8}$$

B. Pre-distortion Computation

Once the metrics for $\mathbf{X_{DT}}$ have been computed, they serve as the basis for determining the pre-distortion values. These metrics also provide crucial information about which input symbols ($a_{(k,l)}$) should undergo how much distortion and the direction of such distortion. A negative metric value implies that the corresponding sample should be distorted toward the origin, while a positive metric value indicates that the corresponding sample should be distorted away from the origin.

The computation of the pre-distortion value for each sample of $\mathbf{X_{DT}}$ involves utilizing the metric calculated for that specific sample, its root-mean-squared power, and adherence to the EVM constraint. The proposed method for computing the amplitude of the pre-distortion value is outlined as follows:

$$d_{k,l} = \left(\frac{\epsilon_{\text{rms}}}{\sqrt{\frac{1}{M}\sum_{l=0}^{M-1}\mu_{k,l}}}\right)\mu_{k,l}. \tag{9}$$

In addition to the scaling presented in Eq. (9), the direction of the distortion should align with the considerations mentioned above. The proposed formulation ensures that the pre-distortion values are calculated based on the metric, normalized by the root-mean-squared power of the corresponding sample, and scaled according to the prescribed EVM constraint. Consequently, this approach not only takes into account the directional information provided by the metrics but also ensures compliance with the available EVM limits.

Upon the computation of all pre-distortion values $d_{k,l}$, a pre-distortion sample matrix in the DD domain is obtained, denoted as $\mathbf{P_{DD}}$. To seamlessly integrate these pre-distortion values with the original DT signal ($\mathbf{X_{DT}}$) and achieve an OTFS waveform with reduced PAPR values, an IDFT is applied to $\mathbf{P_{DD}}$, transforming it into the DT domain. The expression for the final OTFS waveform with reduced PAPR is shown in the following.

$$\mathbf{Y_{DT}} = \mathbf{X_{DT}} + \mathbf{P_{DD}}{\mathbf{F_M}}^{\mathbf{H}}. \tag{10}$$

C. Remarks on Metric Computation

In our proposed metric computation, we utilize both real and imaginary projections of each input information symbol on the samples in the DT domain. It allows us to assign different pre-distortion values to real and imaginary components in each information symbol, which gives us an additional degree of freedom (DoF) to reduce PAPR. To this end, we redefine Eq. (8) for real ($\Re(a_{k,l})$) and imaginary ($\Im(a_{k,l})$) parts separately in the following.

$$\begin{aligned}{\mu^r}_{k,l} &= -\text{sign}(\Re(a_{k,l}))\Re\left\{\sum_{m=0}^{M-1}b_{k,m}|b_{k,m}|^{p-1}e^{-j2\pi lm/M}\right\},\\ {\mu^i}_{k,l} &= -\text{sign}(\Im(a_{k,l}))\Im\left\{\sum_{m=0}^{M-1}b_{k,m}|b_{k,m}|^{p-1}e^{-j2\pi lm/M}\right\}.\end{aligned} \tag{11}$$

where $\text{sign}(\cdot)$ represents the sign function. In Eq. (11), $\sum_{m=0}^{M-1}b_{k,m}|b_{k,m}|^{p-1}e^{-j2\pi lm/M}$ is the Discrete Fourier Transformation on $b_{k,m}|b_{k,m}|^{p-1}$. Computation of complex metrics involves four steps, which can be summarized as follows;

1) Compute matrices W_r and W_i, which contains the directional information for the metric, by performing operation $\text{sign}(\Re(\cdot))$ and $\text{sign}(\Im(\cdot))$ on each element of $\mathbf{X_{DD}}$.
2) Compute a weight matrix W_b by performing operation $|.|^{p-1}$ on each element of $\mathbf{X_{DT}}$.
3) Compute $\mathbf{Z} = (\mathbf{X_{DT}} \odot W_b)\mathbf{F_M}$.
4) Compute matrices: $\mu^r = -W_r \odot \Re(\mathbf{Z})$ and $\mu^i = -W_i \odot \Im(\mathbf{Z})$.

Here, $\odot$ denotes the Hadamard product, and with some abuse of notation we define $\Re(\mathbf{Z})$ and $\Im(\mathbf{Z})$ as the matrices of real and imaginary parts, respectively.

After computation of both the metrics (real/imaginary), we scale them individually and adjust direction for each pre-distortion sample based on information symbol and obtain pre-distortion samples for both the real and imaginary components. It is important to note that both real and imaginary pre-distortion samples should be scaled by $\frac{\epsilon_{rms}}{2}$ to ensure complex pre-distortion remains constrained to ϵ_{rms}.

D. Complexity

In OTFS processing, we can directly transform the input information symbol ($\mathbf{X_{DD}}$) into DT domain samples ($\mathbf{X_{DT}}$) by applying a single IDFT of length M. This entire process incurs a cost of only M-IDFT on N rows $O(NM^2)$. The additional complexity of metric-based CCS algorithm is $O(2NM^2 + 4NM)$, where the dominant term is $O(2NM^2)$ due to DFT and IDFT involved in metric and pre-distortion computations. Furthermore, DFT/IDFT can be efficiently computed using FFT/IFFT algorithm, reducing M^2 term to $M\log(M)$ in overall complexity equation.

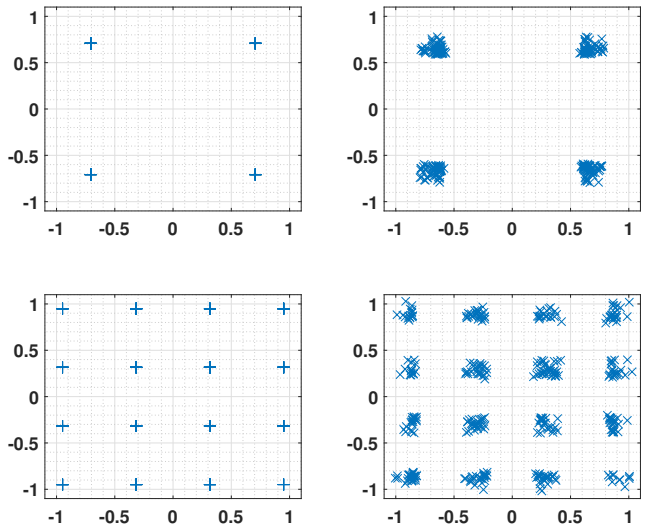

Fig. 3: Ideal and distorted symbol constellation in QPSK and 16-QAM modulation: (left) ideal symbol constellation in OTFS frames, (right) distorted symbol constellation in the metric based CCS algorithm.

IV. Evaluation

In this section, we evaluate our proposed metric based CCS method for PAPR reduction for OTFS. We demonstrate and discuss the PAPR reduction capability of our algorithm and its impact on the BER performance of the OTFS waveform.

A. Simulation Setup

We consider a complex baseband OTFS waveform with QPSK and 16-QAM modulation for $N = 8$ delay-bins and $M = 16/32/64$ Doppler bins. We simulate OTFS frames for different M values to showcase how the PAPR of OTFS increases with an increase in the OTFS frame size. To this end, through simulations, we show that our proposed scheme effectively reduces the PAPR even for large OTFS frames. In simulation, 10^5 OTFS frames are randomly generated and the output samples are over-sampled by a factor of 8. Oversampling is performed here in post-processing to ensure the discrete PAPR values are a good approximation of the continuous PAPR values.

For the proposed algorithm, we compute metrics separately for the real and imaginary parts as defined in Eq. (11). For metric computation $p = 5$ is used (unless mentioned otherwise) as parameter to control the weighing function and the EVM_{rms} threshold for distortion computation is chosen as -15dB and -20dB for QPSK and 16-QAM symbols respectively. The choice of p is computed empirically and EVM_{rms} is set in accordance with the IEEE 802.11ax [18].

Fig. 3 are obtained from a random OTFS frame, with and without pre-distortion to demonstrate the ideal and distorted constellation (after pre-distortion) for QPSK and 16-QAM.

B. Simulation Results

In Fig. 4 we present the CCDF curves for PAPR for both OTFS and OTFS-CCS waveforms across three different weight

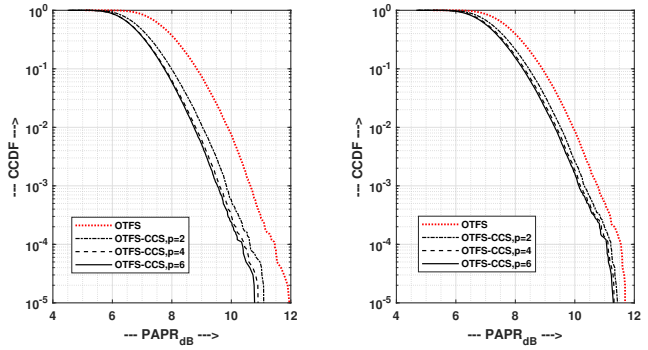

Fig. 4: CCDF curves for PAPR for OTFS and OTFS-CCS waveforms: (left) QPSK modulation, (right) 16-QAM modulation.

configurations. We observe that an increase in the parameter p correlates with a higher PAPR reduction, evident in both QPSK and 16-QAM modulation schemes, while adhering to a predefined EVM constraint (EVM = -15 dB for QPSK and -20 dB for 16-QAM). However, it is noteworthy that the PAPR values exhibit diminishing reductions beyond a certain value of the parameter p. This behavior can be attributed to the influence of the metric, a weighted sum projection of symbols in the DD domain and samples in the DT domain, which is influenced by the value of p. Specifically, a higher p value amplifies the projection for peak-samples compared to the samples corresponding to non-peak samples. This observation underscores the nuanced relationship between the choice of p and its impact on the effectiveness of PAPR reduction in the context of the proposed metric-based constellation shaping method.

Fig. 5 shows that our proposed CCS method effectively reduces the PAPR of the OTFS waveform for both QPSK and 16-QAM modulation schemes. To this end, a notable observation is that the PAPR reduction in QPSK is relatively higher than that observed in 16-QAM. This is because of the more stringent EVM constraints associated with higher-order modulation schemes (-20dB for 16-QAM and -15dB for QPSK). Consequently, these tighter EVM constraints limit

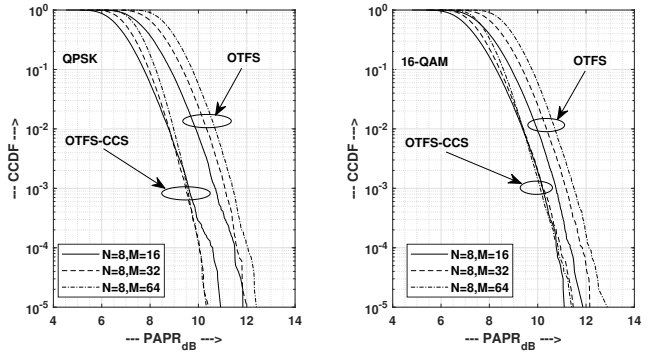

Fig. 5: CCDF curves for PAPR for OTFS and OTFS-CCS waveforms for different OTFS frame sizes: (left) QPSK modulation, (right) 16-QAM modulation.

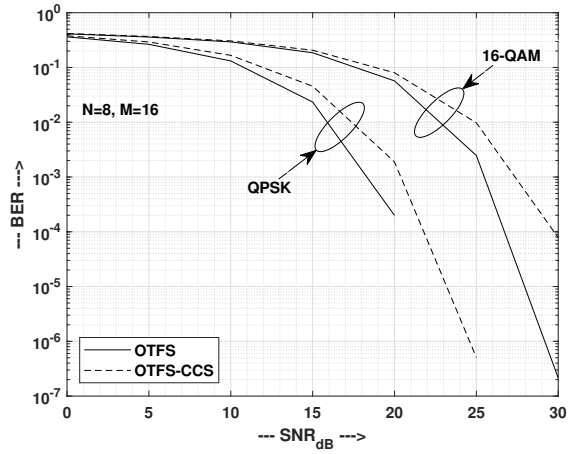

Fig. 6: BER vs SNR performance for OTFS Waveforms with QPSK Symbols. It can be observed that proposed method does add distortion to OTFS Frames, which leads to increase in bit-errors moderately.

the amount of pre-distortion that can be added in a frame to achieve PAPR reduction. We also observe that as the number of Doppler bins (M) increases, the PAPR also exhibits an upward trend. Additionally, our proposed CCS scheme demonstrates increased robustness with an expanding OTFS frame size, due to the fact that, for any OTFS frame of dimension $N \times M$, we have NM samples, which represent the DoF available for metric calculation and to add pre-distortion. As M increases, the added DoF result in more refined metric computation and a robust distortion mechanism, further enhancing the effectiveness of our CCS scheme.

Fig. 6 shows the trade-off associated with the CCS scheme in terms of the BER performance of OTFS modulation. While our scheme successfully reduces the PAPR of the OTFS frame, it requires a slightly higher SNR to attain an equivalent BER performance as that of the original OTFS frame. This observation highlights the inherent compromise between reducing PAPR and the resulting impact on the SNR requirements for maintaining reliable communication. To this end, Fig. 6 serves as a valuable metric for evaluating the performance implications of our proposed CCS scheme, providing insights into the balance between PAPR reduction and the associated SNR requirements in the context of OTFS modulation. This insight empowers the system designer to strategically lower the PAPR whenever the SNR margin permits reduction, all while adhering to the specified EVM limit. Nevertheless, in instances where the BER surpasses a pre-defined threshold owing to an elevated EVM, the designer is compelled to make decisions such as increasing the transmit power, employing different modulation and coding scheme, or refraining from further PAPR reduction.

V. Conclusion

This paper presented a novel metric-based symbol pre-distortion algorithm for reducing the high PAPR associated with OTFS modulation. The proposed method leverages EVM constraints, providing a pragmatic approach that aligns with established wireless standards without introducing additional side-channel information. By using the proposed metrics formulation, the algorithm accurately determines the pre-distortion values for each symbol in an OTFS frame, addressing their individual contributions to peak values in the output. Our simulation results validate the effectiveness of the proposed method, showcasing a substantial reduction in PAPR (up to 2 dB) for both QPSK and 16-QAM modulation schemes. Additionally, the proposed constrained constellation shaping method demonstrates superior performance in PAPR reduction as the number of Doppler bins increases for a given OTFS frame size.

Acknowledgment

This research work was supported by the Spanish Ministry of Economic Affairs and Digital Transformation under European Union NextGeneration-EU projects TSI-063000-2021-59 RISC-6G and TSI-063000-2021-63 MAP-6G. Syed Waqas Haider Shah work was supported by MSCA-PF project RISE-MM (101061011) funded by the European Union Horizon Europe program.

References

[1] R. Hadani, S. Rakib, M. Tsatsanis, A. Monk, A. J. Goldsmith, A. F. Molisch, and R. Calderbank, "Orthogonal time frequency space modulation," in *Proc. IEEE Wireless Communications and Networking Conference (WCNC)*, 2017, pp. 1–6.

[2] K. Zhang, W. Yuan, S. Li, F. Liu, F. Gao, P. Fan, and Y. Cai, "Radar sensing via OTFS signaling: A delay doppler signal processing perspective," in *Proc. IEEE International Conference on Communications (ICC)*, 2023, pp. 6429–6434.

[3] R. M. Augustine, G. D. Surabhi, and A. Chockalingam, "Space-time coded OTFS modulation in high-doppler channels," in *Proc. IEEE 89th Vehicular Technology Conference (VTC2019-Spring)*, 2019, pp. 1–6.

[4] P. Raviteja, K. T. Phan, Y. Hong, and E. Viterbo, "Interference cancellation and iterative detection for orthogonal time frequency space modulation," *IEEE Transactions on Wireless Communications*, vol. 17, no. 10, pp. 6501–6515, 2018.

[5] S. K. Mohammed, R. Hadani, A. Chockalingam, and R. Calderbank, "OTFS—A mathematical foundation for communication and radar sensing in the delay-doppler domain," *IEEE BITS the Information Theory Magazine*, vol. 2, no. 2, pp. 36–55, 2022.

[6] A. Zhou, Y. Pan, J. Wu, H. Lin, and J. Yuan, "On the performance of practical pulse-shaped OTFS with analog receivers," in *Proc. IEEE International Conference on Communications Workshops (ICC Workshops)*, 2023, pp. 518–523.

[7] P. Raviteja, K. T. Phan, Y. Hong, and E. Viterbo, "Orthogonal time frequency space (otfs) modulation based radar system," in *Proc. IEEE Radar Conference (RadarConf)*, 2019, pp. 1–6.

[8] F. Lampel, A. Avarado, and F. M. Willems, "On OTFS using the discrete zak transform," in *Proc. IEEE International Conference on Communications Workshops (ICC Workshops)*, 2022, pp. 729–734.

[9] V. Yogesh, V. S. Bhat, S. R. Mattu, and A. Chockalingam, "On the bit error performance of OTFS modulation using discrete zak transform," in *Proc. IEEE International Conference on Communications (ICC)*, 2023, pp. 741–746.

[10] A. S. Bondre and C. D. Richmond, "Dual-use of OTFS architecture for pulse doppler radar processing," in *Proc. IEEE Radar Conference (RadarConf22)*, 2022, pp. 1–6.

[11] G. D. Surabhi, R. M. Augustine, and A. Chockalingam, "Peak-to-average power ratio of OTFS modulation," *IEEE Communications Letters*, vol. 23, no. 6, pp. 999–1002, 2019.

[12] J. K. Francis, R. Mary Augustine, and A. Chockalingam, "Diversity and PAPR enhancement in OTFS using indexing," in *Proc. IEEE 93rd Vehicular Technology Conference (VTC2021-Spring)*, 2021, pp. 1–6.

[13] A. S. Sümer, T. Yılmaz, E. Memişoğlu, and H. Arslan, "Exploiting OTFS frame structure for PAPR reduction," in *Proc. IEEE 96th Vehicular Technology Conference (VTC2022-Fall)*, 2022, pp. 1–5.

[14] Y. I. Tek and E. Basar, "PAPR reduction precoding for orthogonal time frequency space modulation," in *Proc. 46th International Conference on Telecommunications and Signal Processing (TSP)*, 2023, pp. 172–176.

[15] S. Sezginer and H. Sari, "Metric-based symbol predistortion techniques for peak power reduction in OFDM systems," *IEEE Transactions on Wireless Communications*, vol. 6, no. 7, pp. 2622–2629, 2007.

[16] S. H. Sezginer, S., "OFDM peak power reduction with simple amplitude predistortion," *IEEE Communications Letters*, vol. 10, no. 2, pp. 65–67, 2006.

[17] S. Sezginer and H. Sari, "Peak power reduction in OFDM systems using dynamic constellation shaping," in *Proc. 13th European Signal Processing Conference*, 2005, pp. 1–4.

[18] "IEEE Standard for Information Technology–Telecommunications and Information Exchange between Systems Local and Metropolitan Area Networks–Specific Requirements Part 11: Wireless LAN Medium Access Control (MAC) and Physical Layer (PHY) Specifications Amendment 1: Enhancements for High-Efficiency WLAN," *IEEE Std 802.11ax-2021 (Amendment to IEEE Std 802.11-2020)*, pp. 1–767, 2021.